Arab J Geosci (2015) 8:6465–6482
DOI 10.1007/s12517-014-1711-5

ORIGINAL PAPER

Morphometric analysis of landslides in the Ouarsenis area (west Algeria): implications for establishing a relationship between tectonic, geomorphologic, and hydraulic indexes

Zaagane Mansour · Benhamou Miloud · Frédéric Donzé · Refas Soraya · Hamimed Abderahmane

Received: 22 May 2014 / Accepted: 4 November 2014 / Published online: 18 November 2014

Abstract Ouarsenis mountain range located in the NW of Algeria is affected by numerous slope instabilities: (i) rock falls, related to Jurassic limestone formation and (ii) landslides initiated on moderate slopes angles ranging from 11 to 22 %, which can be related to very sensible lithology (colluviums and turbidity). These slopes show an important fluid circulation activity. This circulation is ensured by a complex karstic system embedded within the limestone mountains in high altitude (>900 m). The rose diagrams establishing of faults lineation, landslides, and elongate slope axis show a strong coincidence between the tectonic fractures and the rupture axis (RA) of the landslides (N10°, N40°, N120°, N140°). The orientations of elongate slope axis coincide mainly with the directions ~N30° and ~N160. The north slopes are affected by a high number of identified landslides because these mountain sides correspond to wetland areas. The topographic and border conditions can highly control the geometry of the landslides: the type of slope and the spread in length of the destabilized materials are strongly related. This is confirmed by the possible linear fit which links the mobility index to the maximum length of the landslides, either with fluid flow or situated in the front of tectonics overlap; these two types of landslides are characterized by low coefficients of friction 0.23 and 0.24, respectively. The landslides situated above the geomorphologic knickpoint are represented by a higher friction coefficient (0.25), as well as landslides initiated in zones without seepage water (0.29): these different apparent friction values can explained the spread in length variability of the debris. Moreover, the high landslide zone is located near a seismic area which can be related to an active deformation process associated to seismogenic faults (e.g., the earthquake which occurred in the Chlef area in October 1980).

Keywords Ouarsenis · Tectonic fractures · Slope instabilities · Fluid flow · Landslide · Friction

Z. Mansour (✉) · H. Abderahmane
Laboratoire de Recherche sur les Systèmes Biologiques et la Géomatique (LRSBG), Université Mascara, Route de Mamounia, MascaraBP: 305, 29000, Algérie
e-mail: zaagane@yahoo.fr

R. Soraya
Université Mascara, Route de Mamounia, MascaraBP: 305, 29000, Algérie

B. Miloud
Laboratoire de Géodynamique des Bassins et Bilan Sédimentaire (GéoBaBiSé), Université Es-senia, Oran, PO Box 1524, El M'naouer, Oran 31000, Algérie

F. Donzé
University Grenoble Alpes, F-38000 Grenoble, France

Introduction

The northern fringe of Algeria is occupied by mountainous system called Tellian range. This structure is subdivided into different structural zones. These include (i) the internal domain represented mainly by limestone range of Kabylie (Durand Delga 1969; Raoult 1974; Bouillin et al. 1970), (ii) an intermediate flysch zone (turbidities) (Blès 1971; Kireche 1993), and (iii) an external zone consisting in thrust nappes essentially (Benaouali-Mebarek et al. 2006).

The Tellian basin supports a thick series of allochthonous layers called "Tellian nappes," which are gravity-driven nappes forming a complex imbricated fan from a lithostratigraphic point of view: these nappes are formed from Upper Cretaceous to Lower Miocene series (Wildi 1983) (Fig. 1a). On the north side of the Tellian range, the decollement flooring the Tell nappes rests upon the large

east-trending imbricated stack of south-directed thrusts made up of Jurassic to Albian strata (Benaouali-Mebarek et al. 2006). These imbricated strata constitute the former substratum of the Tellian nappes that were detached from it along under-compacted and over-pressured horizons located at the top of the Albian strata (Benaouali-Mebarek et al. 2006). This Tellian part is the seat of strong neotectonic activity; this is confirmed by an important number of earthquakes affecting this area (Meghraoui and Pondrelli 2013) (Fig. 1a).

As elsewhere in the Tell zone, the Ouarsenis region is affected by Neogene tectonics (Zaagane et al., Comptes Rendus of Geoscience, under review); it results in (i) imbricate tectonic nappes on the northern part, which is due to a paroxysmal tectonic phase upper Miocene in age and the affected lands range from the upper Cretaceous to Miocene, (ii) an extrusion of structural units along neoformed faults in relation to the first tectonic phase that affected the Ouarsenis, and (iii) a late deformation of the structural units as a result of compressive ENE/WSW constraint along a right strike slip oriented in a N120° direction (Fig. 1b). The Ouarsenis area, which forms a part of the external Tellian domain of Algeria, is located at 170 km SW from Algiers. This region elongates about 120 km^2, and it is composed of the following: (i) Sra Abdelkader, elongating from west to east for 4 km and culminating at 1,760 m, (ii) the Grand Pic range culminating at 1,985 m, (iii) Rokba Atba culminating at 1,200 m, and (iv) Belkheiret elongates from NNE to SSW and culminating at 1,620 m. This mountain range is located in the south of the Ouarsenis zone, and it is oriented in a NNE-SSW direction (Fig. 2a). To this main region, satellite mountain ranges including Kef N'sour, Batha, Fartas, and the Chicots massifs can be added (Fig. 2a).

This overall morphology is the result of complex and multiphase tectonic processes. Indeed, tectonic stress alternating from NW-SE to NE-SW directions has given rise to steep relief along the overlapping lines. These structures originated from two folding phases P1 and P2 which are oriented in NW/SE and NE/SW directions, respectively; both are probably Tortonian and Pliocene age (Zaagane et al., Comptes Rendus of Geoscience, under review). The now disappeared Triassic formation has played the role of detachment surface for the carbonate formations belonging to the Jurassic age. This material was extruded along abnormal contacts (Fig. 2b). Therefore, these important constraints have exhumed the underlying material represented by Jurassic formations at high altitudes (>1,000 m) (Fig. 2b). However, the lower elevations are represented by a ductile material that still surrounds the limestone islet (Fig. 2b). A colluvium material overcomes the Mesozoic series; it presents a vulnerable character for land movements where the forest is lacking. The gravitational instabilities on catchment areas are related to a complex morphotectonic process (Maquaire et al. 2004; Thiery et al. 2004, 2007). These movements share common triggering and predisposition features, which include displacement under gravitational effect from destabilized materials by either natural or anthropogenic factors (intense precipitation, seismicity, deforestation, or mining development and farming. To understand the spatiotemporal character of triggered landslides (Thiery et al. 2004), two approaches have been developed: (i) analytical methodologies involving probability of occurrence of landslides with a multivariate statistical approach (Carrara et al. 1991), (ii) mathematical approaches (logic fuzzy, evidence theory, neural network, etc.) which highlight susceptibility maps of hazard instability (Carrara et al. 2003; Thiery et al. 2007).

Dynamic predisposition parameters have been at the origin of the majority of landslides triggering and they can listed such as the following: (i) the induced fracturing, (ii) the direction and gradient of slopes, (iii) the nature of the involved materials, and (iv) the fluid circulation. They are considered to be the main features that accommodate not only triggering but also the direction of the gravity flow (Lucas and Mangeney 2007; Lucas et al. 2007, 2008). The role of the shape of the slopes is also important in the stability. Since the morphology of the slopes varies widely, rectilinear, concave, convex, concave-convex, or convex-concave geometries can be involved (Lebuis et al. 1983). These slopes are the direct consequence of the structural nature of the area. There are two types of geomorphologic knickpoints which can be characterized by either their morphological positions or their tectonic positions (Fig. 2c). In all cases, the rupture slope located on the foreheads of overlaps has a chaotic character. They coincide with a lithological unconformity due to the passage of the overlap path. This line is located between 1,300 and 1,400 m elevations for the Belkheiret (FF′), Batha (II), Grand Pic (DD″), and Sra Abdelkader (HH′) cases. They are not as high as what can be observed in the other ranges (Fig. 2c).

However, the slopes of rear part of these overlaps are long with a concave shape (Fig. 2c). These knickpoints are located within the elevation levels between 1,200 and 1,300 m. Exception is made for the eastern extremity of Sra Abdelkader where this limit is about ~950 m. The location of the knickpoints totally depends on the tectonic signature combined to clastic superficial phenomena (Lebuis et al. 1983).

Depending on the properties of the slope (lithology, slope angle, hydraulic gradient, and parameters related to the shear strength), the factors of instability are calculated in different manner and the resulting values can very different (Lebuis et al. 1983). For examples, for rectilinear slopes, concave-convex, or convex, the obtained safety factor value is higher than the one calculated for concave or convex slopes, whereas it is lower for concave slopes (Lebuis et al. 1983). Considering the topography of this region, two main types of slope geometry can be listed: concave and convex-concave geometries. These slope types can also have different lengths as observed

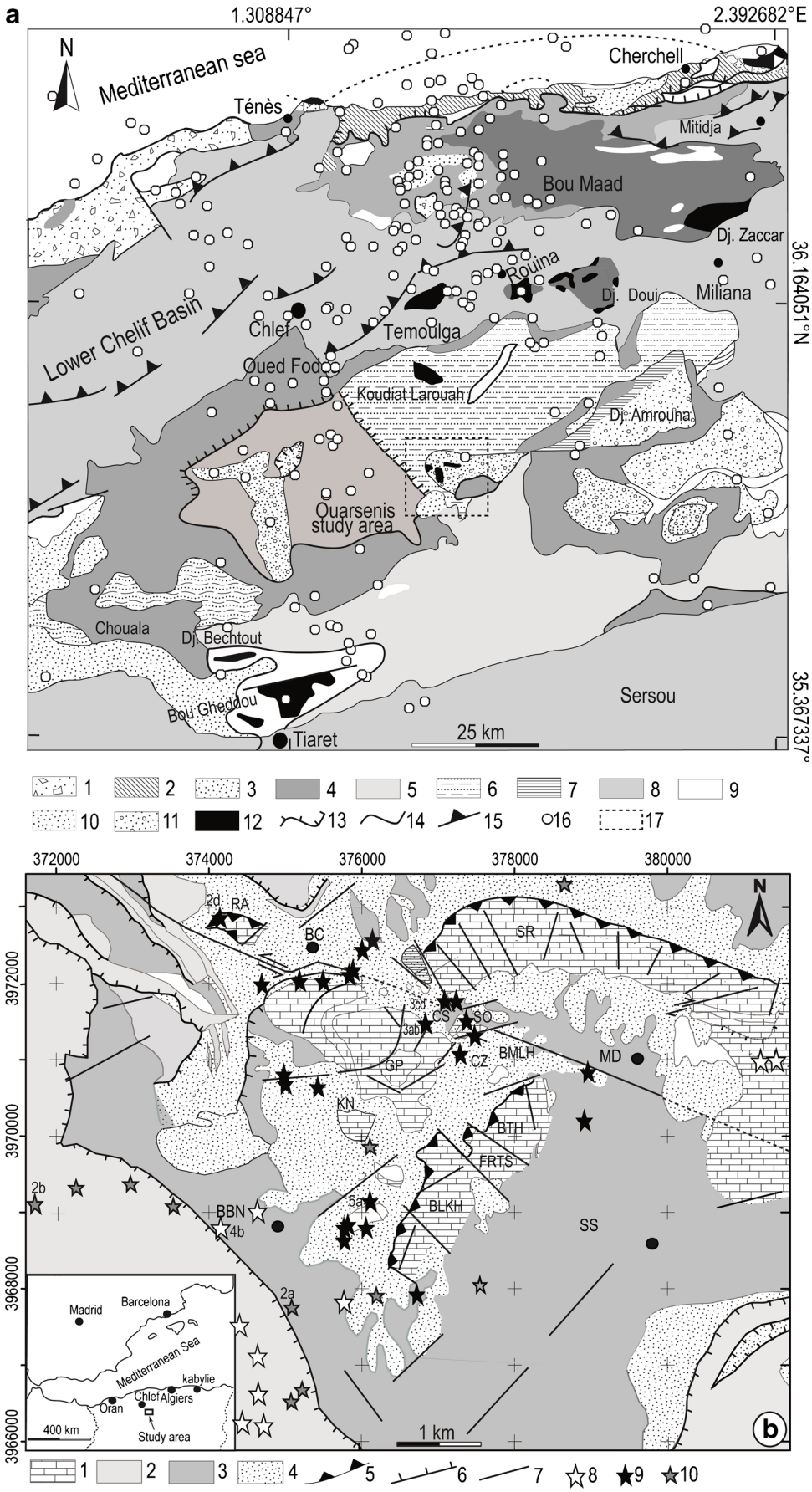

Fig. 1 Structural characters of the study area. **a** Map showing a stack of nappes in a part of the external domain: *1*, Numidian nappe; *2*, turbidities nappe; *3*, sub-Numidian nappe; *4*, epi-Tellian nappe; *5*, South-Tellian nappe; *6*, infra-Tellian nappe; *7*, sedimentary klippen; *8*, post-Miocene formation; *9*, Miocene; *10*, Cenomanian to Paleocene; *11*, Lower Cretaceous; *12*, Jurassic; *13*, major tectonic contact; *14*, main fault; *15*, active fault; *16*, earthquake; and *17*, study area. **b** Structural map of the Ouarsenis culminating zone (UTM. WGS84 projection): *1*, Jurassic limestones basements; *2*, tectonics nappe; *3*, Albo-Aptian flyschs; *4*, recent covering; *5*, abnormal tectonic; *6*, tectonics nappe limits; *7*, hypothetic faults; *8*, natural landslide; *9*, landslide related to tectonic events; *10*, landslide generated by road traffic. The various structural units are represented by *SR* Sra Abdelkader, *RA* Rokba Atba, *BTH* Batha, *FRTS* Fartas, *GP* Grand Pic, *BLKH* Belkheiret, *BMLH* Bou Malah, *SO* Sidi Ouadhah, *CS* Senan pass, *MC* Chicots massif, *KN* Kef N'Sour, *R* Roubia, *CZ* central zone, respectively. The code corresponds to the location of figure numbers

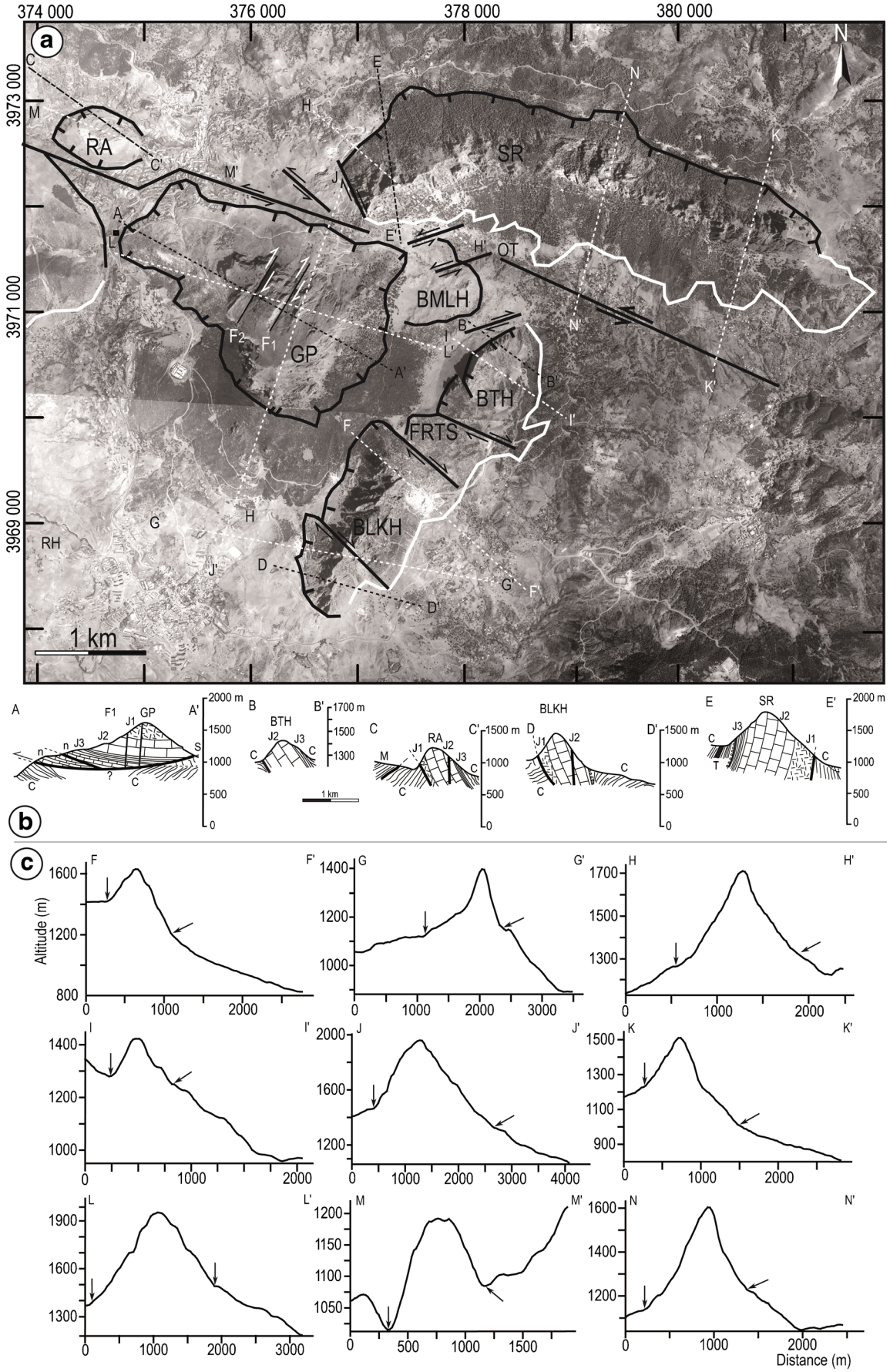
374 000
376 000
378 000
380 000
3973 000
3971 000
3969 000
a
N
RA
SR
BMLH
GP
BTH
FRTS
BLKH
QT
RH
F2
F1
1 km
b
c
Altitude (m)
Distance (m)

◀ **Fig. 2** **a** Aerial map composed of 20 views on a 1:20,000 scale (UTM WGS84) showing the location of the study area among the structural units of the Tellian domain. *R* Roubia, *RH* Resfat Halayeg, *OT* Oued Tesrine. *White (black) dashed lines* represent the topographic and geological profiles, respectively. *Black lines* refer to nick line of slope bound to the tectonic contacts; *white lines* refer to nick line of morphologic slope. F1, F2: dextral faults. 1–46: landslide gravity centers, notice that other landslides are located outside this picture (see coordinates in Table 1); **b** cross sections along the structural units, through the central Grand Pic massif (AA′), the Batha massif (BB′), the small Rokba Atba massif (CC′), the southern part of Belkheiret (DD′), the southern part of Sra Abdelkader (EE′). *T* Triassic, *J1* Lower Liassic, *J2* Upper Liassic, *J3* Malm, *n* Neocomian, *C* Clansayesian-Albian, *S* Senonian, *M* Miocene; **c** topographic profiles along several sections: FF′, GG′, and HH′ in the southern, central, and eastern part of Sra Abdelkader, respectively; II′, JJ′, and KK′ in the southern, northwest, and eastern part of the Grand Pic, respectively; LL′ and MM′ in the southern and northwest part of Belkheiret, respectively; NN′ refers to the northwest of Batha massif. *Vertical arrows*, rupture slope from tectonics; *oblique arrows*, rupture slope from morphology. (For interpretation of the colored references used in this figure legend, the reader is referred to the web version of this article). For the rest of abbreviations refer to Fig. 1

in the south side of Sra Abdelkader and SE Belkheiret region (concave-long types), or the North side of Sra Abdelkader and the western mountain sides of Belkheiret (convex-concave-short) (Fig. 2c).

The morphometric analysis of the in situ characteristics has been the subject of several models in analog environments; these models have been used to explain the role of different parameters such as the coefficient of friction, the length area of displaced material, or equilibrium factor (Mangeney-Castelnau et al. 2005; Mangeney et al. 2007). A key morphometric parameter is often used in kinematic analysis of landslides: the mobility index landslide (H/L), where H and L are the height difference and the horizontal length of the landslide from the rupture zone, respectively (Scheidegger 1973; Hsü 1975). Other authors have studied the effects of topography on the H/L ratio for shallow landslides (Finlay et al. 1999; Hunter and Fell 2003; Okura et al. 2003). Rather than using this parameter, some authors have used the horizontal length of the accumulation zone as a key parameter (Mangeney-Castelnau et al. 2005; Mangeney et al. 2007). This last parameter is also used in geological studies related to rock avalanches: in this case, it is called the effective friction (Mangeney et al. 2007). It represents the ratio between the initial height rupture (Hi) and the maximum distance traveled by the avalanche (Lf) (Lucchitta 1987; Dade and Huppert 1998; Guthrie and Evans 2004; Mangeney-Castelnau et al. 2005).

In this context, the present work focuses on the following:

(i) Establishing a correlation factor between the disposition features (fracture orientation, slope gradient, and fluids flow) and the induced phenomena (rupture surfaces, gravitational movement of the material, and morphology of generated landslides). It includes the determination of the relative importance of trigger factors the slope movement.

(ii) Analysis of the in situ morphometric parameters for different cases studies, to infer the effects of the morphology and fluids flows on the friction factor.

Investigated area and landslide events

Geological and setting

The geology of the Ouarsenis area is characterized by Mesozoic landscapes (Glangeaud 1951; Calembert 1952; Mattauer 1958; Tchoumatchenco et al. 1995; Benhamou 1996). The Jurassic formations are represented by a competent material which includes limestone and dolomitic limestone alternating locally with marl limestone or sandstone levels (Mattauer 1958; Farès Khodja 1968; Kireche 1993; Benhamou et al. 2000; Elmi et al. 2003). These formations are located on the higher elevations and are subject to thermoclastic and chemical disaggregation. They overlap the cretaceous formations (Mattauer 1958) (Fig. 2b). The curvilinear faults bordering structural units are marked by Triassic uplifts and contain fragments belonging to the Paleozoic bedrock (Mattauer 1958).

These formations were extruded under the effect of alpine constraints oriented in the NW-SE and NE-SW directions, Tortonian and Pliocene in age, respectively. The first stress loading has generated the folding and overlying, whereas the final stress loading phase is responsible of a sinisterly shearing strike slip oriented ~N120° (Zaagane et al., Comptes Rendus of Geoscience, under review). The overlying land is composed of a ductile limestone-marl alternation material type, Neocomian in age, or Albo-Aptian turbidities (Glangeaud 1951; Polvèche 1960; Benhamou 1996) (Fig. 2b). These marl quartzite series belong to the tectonic nappes denominated nappes A (Mattauer 1958). The Cenozoic land is located in the north and south of the culminating zone of Ouarsenis (Atrops et al. 1991).

The formations belonging to these stages are characterized by gray marl and carbonate terraces. Their establishment is related to the late regression of Calabrian Sea (Mattauer 1958). The existence of sometimes combined strike-slip faults, stretching out on 4–5 km in length, is a clear boundary between two different materials: (i) competent (Liassic limestone) and (ii) ductile (turbidities). The evolution of the different culminating zones of Ouarsenis suggests that they have undergone significant displacement (sample of Rokba Atba which translocate 2 km to the NW): this a direct consequence of middle phase characterized by an extensional phase in the WNW-ESE direction (Zaagane et al., Comptes Rendus of Geoscience, under review). On the overall mountain range, the dips of the Mesozoic formations are sub-orthogonal,

compared to lines of the tectonic faults, except for the Grand Pic zone (Fig. 2b). The Dogger and Malm formations are mainly oriented N60°, with an average dip of 70° SSE in the Rokba Atba zone (Dalloni 1936; Mattauer 1958; Calembert 1952); they become ~N20° in the southern massifs (Belkheiret and Fartas Batha areas). In Sra Abdelkader, the same formations are ~70° inclined to the south direction with a ~N100° orientation (Fig. 2b). In the para-autochtonous zone of the Grand Pic, the formations dating from the Lower Liassic to Cretaceous are sub-horizontal with a slight inclination (<10°) to the east (Calembert 1952) (Fig. 2b). However, at low altitude, the Albo-Aptian formations are more ductile and they tilt towards the SW direction.

The location of tectonic knickpoints is related to the appearance of their topography catchment. Indeed, the rupture due to the presence of a fault corresponds generally to an abrupt change of slope gradient, reminding that the objective of the present study is to identify this type of slope (convex/concave and concave such as the following: non-homogeneous slopes having chaotic characteristics correspond to the convex-concave geometries (e.g., on the western slopes of the Belkheiret zone (GG′) (Fig. 2c)), whereas the slopes related to the disposal morphology are more concave (e.g., on the southern side of Sra Abdelkader zone (NN′) (Fig. 2c)). The instability is relatively different for each type of slope, i.e., (i) 0.75 for the western part of Belkheiret and (ii) 0.83 for the southern part of Sra Abdelkader (Table 1; Lebuis et al. 1983).

Climatic aspects

The altitudes ranging between 800 and 1,000 m represent 49 % of the entire studied area, while the 1,000 to 1,200 m constituted by 27 % of this zone. These high altitude zones are covered by snow during the winter season, which can last until May. Therefore, the complex karst system located in the Jurassic limestone (J1–J3) (Fig. 2b) is at the origin of the most downstream sources, which are active all the year long. The lower altitudes (<800 m) cover 24 % of the entire area. They are composed of (i) slightly inclined slopes corresponding to old landslide surfaces (L21) (Table 1) as well as (ii) valleys along lines associated to tectonic weakness like the Tesrine Oued. This overall mountain area is subject to a different climate regime compared to surrounding areas. Recent rainfall data records indicate the existence of a long rainy season extending from November to March, and a short dry season extending from May to October. The seasonal average value of rainfall is completely different between the first and the second season with 516.4 and 59.65 mm, respectively. The average rainfall is about ~576 mm/year. Almost the majority of landslides were triggered during the first season. The monthly oscillations can be perturbed by thunderstorm events which are common during the heavy rainfall season (Fig. 3). The intensity of these thunderstorms is variable but they can cause (i) mudflows or (ii) small landslides.

Identified landslides description

The identified landslides within the high-altitude area of Ouarsenis (over 1,000 m) occupy 0.23 % of the total surface (Table 1). However, only instabilities located around the buildings and infrastructure are taken into account. Despite the small extent, they cause considerable damages: (i) ruined houses (Table 1, L10 event), (ii) infrastructure completely destroyed (Fig. 4a, L3 and L5 events), as well as damaged roads causing traffic problems for months (Fig. 4b, c) (Table 1, L36 and L40 events). In their majority, these landslides are superficial and they do not exceed 10 m in depth: as an example, the interpretation of seismic profiles shows that the sliding surface is about 8.5 m deep (Fig. 4a, L5 event). However, the L21 event, located on the SW of the town of Bordj Bou Naama, seems to be deeper, as an important part of the zone is wrenched (Table 1).

Other landslides occurring on the north side of the massif of the Grand Pic as well as the northwest side of the massif of Belkheiret represent 8.3 and 29.94 % of the total landslides, respectively. The affected landscapes are located at altitudes higher than 1,060 m for the Grand Pic area and around 800 m for the Belkheiret zone (Table 2). The landslides located in the front of tectonics knickpoints represent 54.34 %, while those located on concave slopes represent 45.65 % of all landslides identified: typical examples are situated on the south side of Sra Abdelkader (SR) (Table 2). Twenty-four gravitational instabilities can be related to water fluctuations, which represent 52.17 % of the landslides (Table 3). Most of them are located between Belkheiret and Grand Pic zones. Other landslides might be directly related to the influence of tectonics. For example, a tectonic contact marked by a deep reverse fault in the NW part of Rokba Atba (RA) (Fig. 4d). This different structure corresponds to the plane of an overlap. Indeed, the formations of the lower Liassic (J1) overlap the Albo-Aptian flysch units (C) (Fig. 2b). The presence of a boundary fault is the origin of this landslide (Fig. 4d).

From a general point of view, the different recorded events can be classified into four distinct categories: rockfall, translational, rotational, and complex rotational modes.

Rockfalls (RF)

The rockfalls events are mainly localized at altitudes exceeding 1,000 m, and they affect a competent material, in particular Jurassic carbonate rocks. They represent 2.63 % of all reported cases. For example, Calembert (1952) noted a rock collapse on the southeast side of Sra Abdelkader. The debris flow

Table 1 Parameters of the 46 recorded landslides in the Ouarsenis culminating zone

Code	*X* (°N)	*Y* (°E)	L_p	L_t	L_{rz}	L_{df}	*S* (m^2)	AC (m)	*P* (m)	H_i/L_f	ms (%)
L1	35.8834	1.62095	183.26	190.37	58.02	130.84	9,365.51	24.00	441.43	0.13	18
L2	35.8411	1.61231	47.32	58.28	1.00	46.00	3,486.11	19.00	241.20	0.40	41
L3	35.8560	1.62391	115.60	129.20	3.00	110.00	2,922.47	28.00	296.56	0.24	25
L4	35.8546	1.62392	142.93	169.19	1.00	141.93	9,385.07	45.00	418.56	0.31	32
L5	35.8830	1.61219	163.63	169.03	23.95	140.00	16,699.57	22.00	544.25	0.13	16
L6	35.8760	1.68313	18.99	19.86	1.50	17.50	1,034.89	3.00	188.33	0.15	17
L7	35.8969	1.65527	53.91	56.57	2.00	51.91	3,708.54	8.00	337.25	0.14	15
L8	35.8761	1.68531	23.16	24.37	2.00	21.16	1,348.42	4.00	259.87	0.17	19
L9	35.8375	1.60604	187.15	187.23	19.05	168.18	18,632.01	56.00	631.94	0.30	33
L10	35.8446	1.60984	80.50	81.23	19.01	60.00	6,082.25	13.00	308.74	0.16	22
L11	35.8613	1.59372	71.24	75.59	3.00	68.24	2,983.96	13.00	213.54	0.18	19
L12	35.8591	1.59974	69.38	74.94	2.00	67.38	3,167.98	14.00	213.21	0.20	21
L13	35.8365	1.61153	18.37	19.83	1.50	16.96	541.75	3.00	119.16	0.16	18
L14	35.8328	1.61235	29.64	31.78	2.00	27.64	1,069.95	5.00	128.75	0.16	18
L15	35.8332	1.60952	85.33	96.84	27.25	58.00	12,935.86	23.00	648.61	0.27	40
L16	35.8559	1.60624	15.59	18.20	2.00	13.59	1,581.81	5.00	279.51	0.32	37
L17	35.8462	1.61582	27.58	31.05	5.94	21.00	1,562.63	7.00	205.85	0.25	33
L18	35.8609	1.58592	56.24	76.13	19.77	36.00	1,721.87	26.00	160.23	0.46	72
L19	35.8731	1.61555	62.50	84.80	3.00	59.50	2,595.57	29.00	195.99	0.46	49
L20	35.8370	1.61797	434.60	687.42	23.80	411.00	43,272.68	263.00	1013.58	0.60	64
L21	35.8356	1.61626	479.16	13.32	20.00	459.00	66,257.12	93.00	1233.53	0.19	20
L22	35.8766	1.64038	42.57	44.88	15.10	27.47	687.14	13.00	103.93	0.30	47
L23	35.8475	1.62706	42.74	44.88	1.00	13.00	1,971.50	16.00	218.10	0.37	23
L24	35.8475	1.63294	141.08	166.57	17.50	123.58	8,995.60	45.00	389.81	0.31	36
L25	35.8829	1.64023	80.78	96.75	10.38	70.40	3,048.20	26.00	251.30	0.32	37
L26	35.8928	1.60626	75.28	87.26	18.20	57.00	4,288.83	22.00	242.76	0.29	39
L27	35.8829	1.63897	17.41	18.88	2.00	15.40	269.66	4.00	62.07	0.23	26
L28	35.8476	1.64050	33.02	35.82	9.03	2.00	1,154.25	7.00	131.28	0.21	50
L29	35.8792	1.63352	30.42	39.21	13.05	17.37	501.42	12.00	86.31	0.39	69
L30	35.8563	1.62450	56.87	58.58	17.03	39.84	2,267.32	7.00	174.37	0.12	18
L31	35.8587	1.57886	23.69	24.47	5.00	18.69	687.90	3.00	102.41	0.12	16
L32	35.8585	1.61163	39.79	58.43	5.00	34.79	1,596.93	8.00	155.97	0.20	23
L33	35.8869	1.62640	40.50	49.70	9.25	31.25	2,334.74	15.00	291.82	0.37	48
L34	35.8841	1.62453	92.75	109.42	15.84	77.09	2,379.68	28.00	251.48	0.30	36
L35	35.8592	1.62755	35.98	41.14	6.48	29.00	977.50	10.00	117.79	0.28	34
L36	35.8727	1.62022	68.02	77.58	2.00	66.02	2,842.73	19.00	216.04	0.28	29
L37	35.8743	1.61532	40.00	151.10	1.00	38.00	5,100.12	5.00	367.61	0.12	13
L38	35.8697	1.65945	52.61	62.15	6.00	46.61	1,889.44	13.00	184.91	0.25	28
L39	35.8473	1.62394	202.07	233.79	15.00	187.07	5,268.71	59.00	480.67	0.29	32
L40	35.8758	1.65862	81.57	92.39	4.00	67.57	1,026.40	22.00	214.40	0.27	33
L41	35.8784	1.64257	57.67	61.61	12.47	47.67	1,649.35	9.00	163.71	0.15	19
L42	35.8810	1.64223	17.57	18.53	3.00	14.57	452.02	4.00	106.55	0.22	27
L43	35.8901	1.62802	57.00	66.96	5.00	52.00	987.11	18.00	156.39	0.31	35
L44	35.8833	1.61762	53.21	59.00	2.00	51.21	2,186.78	11.00	179.50	0.21	21
L45	35.8561	1.62703	40.00	50.00	10.00	30.00	981.01	8.00	139.54	0.20	27
L46	35.8847	1.62519	239.28	286.00	10.00	230.00	11,616.35	79.00	571.14	0.33	34

X, *Y* geographic coordinates, L_p projected distance into the horizontal plan, L_t true distance of the entire landslide, L_{rz} length from rupture zone to the resulting debris flow, L_{df} length of the debris flow, *S* surface, *AC* altitude drop (height difference), *P* perimeter, H_i/L_f friction coefficient (Lebuis et al. 1983), *ms* mean slope

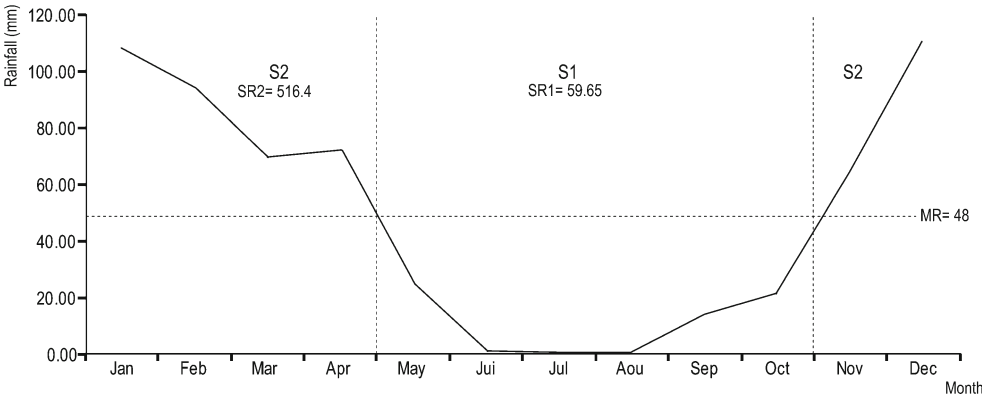

Fig. 3 Diagrams of yearly rainfall activity showing two distinct seasons S1 and S2. The data represent the average value given over 12 years from 1996 to 2008. *MR* corresponds to the monthly average rainfall; *SR1* and *SR2* represent the seasonal average rainfall for the first and the second season, respectively

propagated on the slope overlooking the village of Mitidja. Due to the arrangement of Bajocian limestone in centimetric benches and very straightened with an inclination of ~80° S, these events seem to be mainly linked to a bench to bench slip process. The faults oriented to the N40° (F1 and F2) direction have affected the northern part of the Grand Pic (Figs. 5a and 3b); they have structured this frontage in walking stairs. For example, at the edge of faults (F1), a rockfall occurred recently (Fig. 5c). The debris spread out along the north side of the Grand Pic (Fig. 5d). Two factors seem to be responsible for this rock sliding: (i) the intense fracturing and weakness of the materials along the fault F1 and (ii) the use of explosives for mining purpose nearby (Adushkin 2000). The falling blocks presented large fragment size (Fig. 5e, f). Their fall was

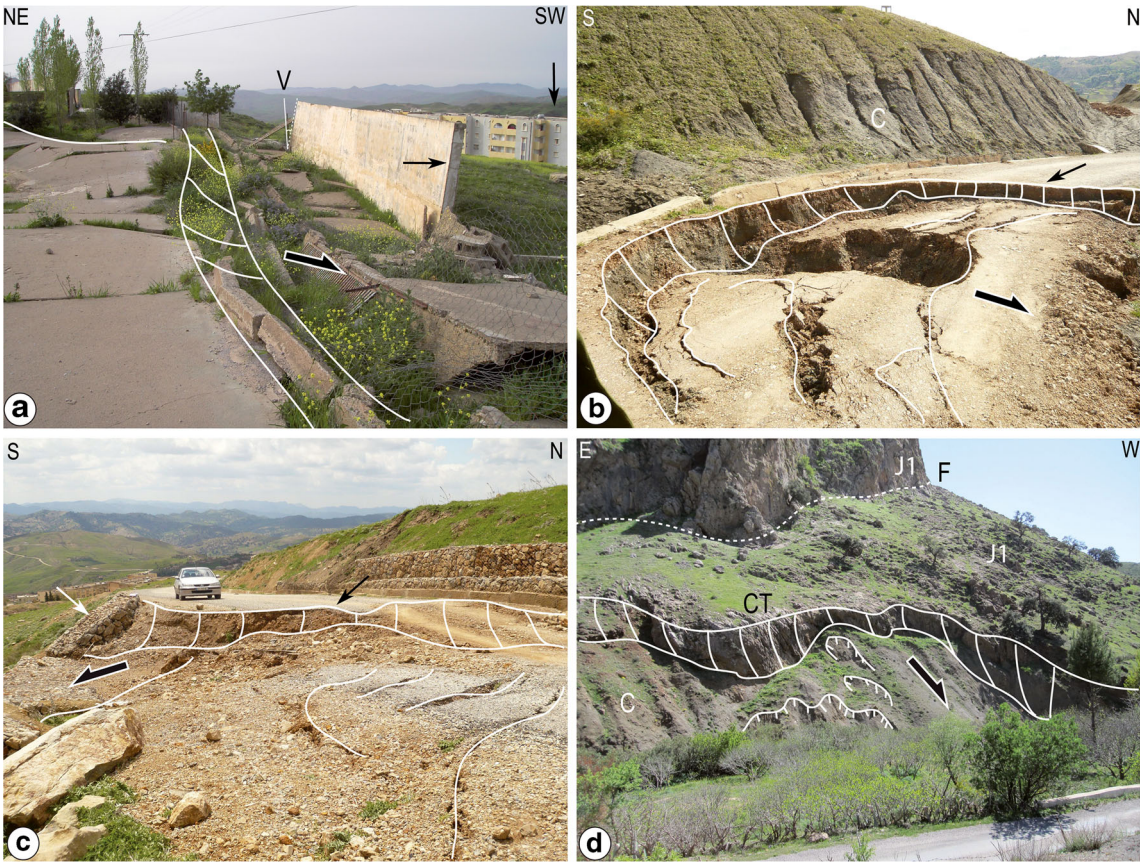

Fig. 4 Photographs showing different types of landslides. **a** Landslide (L5) affecting a stadium and another building below, *V* vertical line reference, *black arrow* showing a wall destroyed and partly tilted; **b** road affected by landslide (L41) west of the Grand Pic isolating people living in the other side; **c** landslide (L12) southwest of Belkheiret affecting colluviums deposits and damaged a new road build 3 years ago, *white arrow* indicates the shift of the concrete barrier; **d** landslide (L33) affected by lithology differentiation limits (for abbreviations code of landslides refer to Table 1.), *CT* tectonic contact, *C* Albo-Aptian flysch, *J1* Liassic limestones, *F* fault, *white lines* rupture area. For abbreviations and location of numbered photos, refer to Fig. 2a

Table 2 Landslide in different areas of the Ouarsenis culminating zone

Area	Geol	Alt (m)	Tl. land (m^2)	Land (%)
SR	CL (Q) with L(J3)	970–1,510	77,504.31	28.1
RA	FL (C)	1,000–1,060	2,334.74	0.85
GP	CL (Q) with L(J1-J2)	1,060–1,640	24,107.79	08.73
BLKH	CL (Q) with FL(C)	800–1,250	81,659.51	29.94
BTH	CL (Q)	1,010–1,040	4,558.49	1.65
RH	CL (Q)	806–1,060	84,817.25	30.73

CL colluviums, *L* limestone, *FL* flysch, *J1* Lower Liassic, *J2* Upper Liassic, *J3* Bajocian, *C* Cretaceous, *Q* Quaternary (see Fig. 2 for abbreviations), *Geol* geological formations affected by landslides event, *Atl* difference in height, *Tl. land* total surfaces of landslides, *Land* (%) the normalized percentage to the entire landslides surface in every massifs

partially caused by subvertical fractures orthogonal to the plane of the main fault F1. On some blocks, tectonic striae in relation to the strike slip movement could be seen (Fig. 5e, f).

The translational landslides (TL)

These kinds of landslides are characterized by a detachment surface of small depth but a large preading area. This type of movement has been identified on the west side above Bordj Bou Naama village (BBN) as well as on the south-east side of the Sra Abdelkader massif. Two examples are shown in Fig. 4a, b, i.e., S-W and west of BBN, respectively (Fig. 6a, b). In the first zone, these movements are favored by a discontinuity between superficial layers (colluviums) and the marly substratum, which represents 39.41 % of this type of cases. In the second zone, the dips of these formations are consistent with the slope and constitute 60.59 % of these landslides. These two types of movement represent 36.95 % of the studied landslides. These include the surface of displaced material which has a length twice its width, as measured on the studied translational slides. They present a complex structure with many geomorphic surfaces of secondary ruptures that spread along the slope (Thiery 2007) (Fig. 6c, d).

The rotational landslides (LR)

These types of landslides are the most represented group in the studied area. They develop along listric plan in the depth direction (Thiery 2007). The rupture surfaces are curved with a depth reaching sometimes dozen of meters (for example, the L21 case). Rotational landslides occur beyond the knickpoint marking the passage of the abnormal contact that surrounds the culminating zone (west of Belkheiret, west and north of Grand Pic, and north of Sra Abdelkader for examples) (Fig. 2b). Recent collapse of the road happening between BBN and Bou Caid (Fig. 7a) has been observed recently. The cross section of these landslides shows that rupture surface is curvilinear and the detachment surface is curved in depth. The disposal area has a dome shape composed of displaced materials accumulation (Fig. 7b). This morphology can be represented by several secondary downstream rupture surfaces from the landslide. This configuration has been reproduced through classical models (Fig. 7c). The analysis of field data shows that this type of rotational landslide represents 60.86 % of the total identified landslides. However, complex rotational landslides located on the edges of the stream courses are only 13.04 %. The landslides characterized by circular failure are generally located in the road cut (Figs. 4b, 5, 6, and 7a).

Methodology

The methodology used to analyze the different landslide's type is composed of three main steps: (1) data collection and construction of a spatial database from the relevant morphometrics index, (2) assessment of the typology of the soil movement using the relationship between the landslide and predisposition factors, (3) validation step by calculating of friction index (Hi/Lf). From this analysis, various methods can be applied to characterize the Factor of Safety (FoS) by studying morphometrics index and the topographic factors (slope). The assessment of the FoS was reviewed by Hattanji and Moriwaki (2009) and Martha et al. (2010).

Landslides in the studied area and inventory

The landslide inventory map provides the geographic locations, the geometrical characteristics, and the outlines of different landslides. Note that no detailed landslide inventory map was previously done for the studied area. Using a Global Positioning System (GPS), the locations of landslide

Table 3 Dynamic parameters of the different types of landslides. Same notations as in Table 1

Dynamic parameters	L_p	L_t	Surface (m^2)	AC (H_i)	P (m)	H_i/L_f	ms (%)
Geomorphology	85.41	102.37	4,169.77	23.60	277.97	0.26	25
Tectonics	55.03	61.66	3,267.58	13.13	223.19	0.24	24
Fluids occurrence	62.02	68.06	3,017.72	13.17	224.23	0.22	23
No fluids	115.43	143.40	9,231.43	38.64	366.34	0.3	29

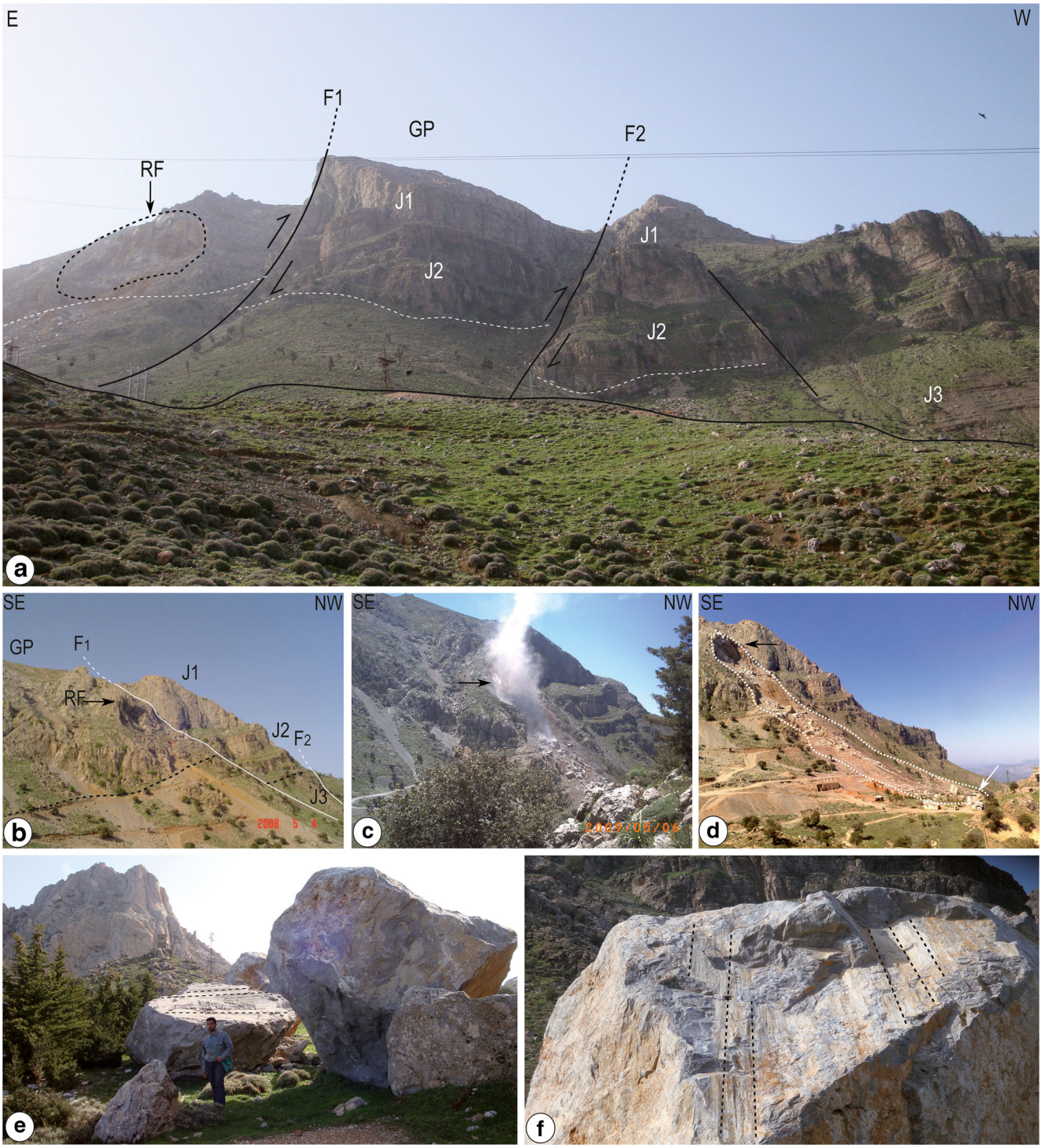

Fig. 5 Photographs showing rock falls (L20) phenomena in the northern part of the Grand Pic. **a** Rockfall relics; **b** live rockfalls with debris flowing over the slopes; **c** same area after the rockfall event; the *dashed white line* represents the area affected by the destabilized materials; **d**, **e** large blocks; the *black dashed lines* represent the striaes of fault F1 (For abbreviations and location of numbered photos, refer to Fig. 2a); and in **d** the *black arrow* shows the starting zone, while the *white arrow* shows the resulting debris zone

were determined and mapped for this investigation, by a field survey since 2008. All parameters related to the areas of landslides were used in the analysis (Hattanji and Moriwaki 2009). Then, these parameters were converted to set up a vector map. A total of 46 landslide points derived from this vector map were used in the analysis. The landslides were then divided into three groups. Twenty-five landslides were identified and the characteristics of some of these slides were

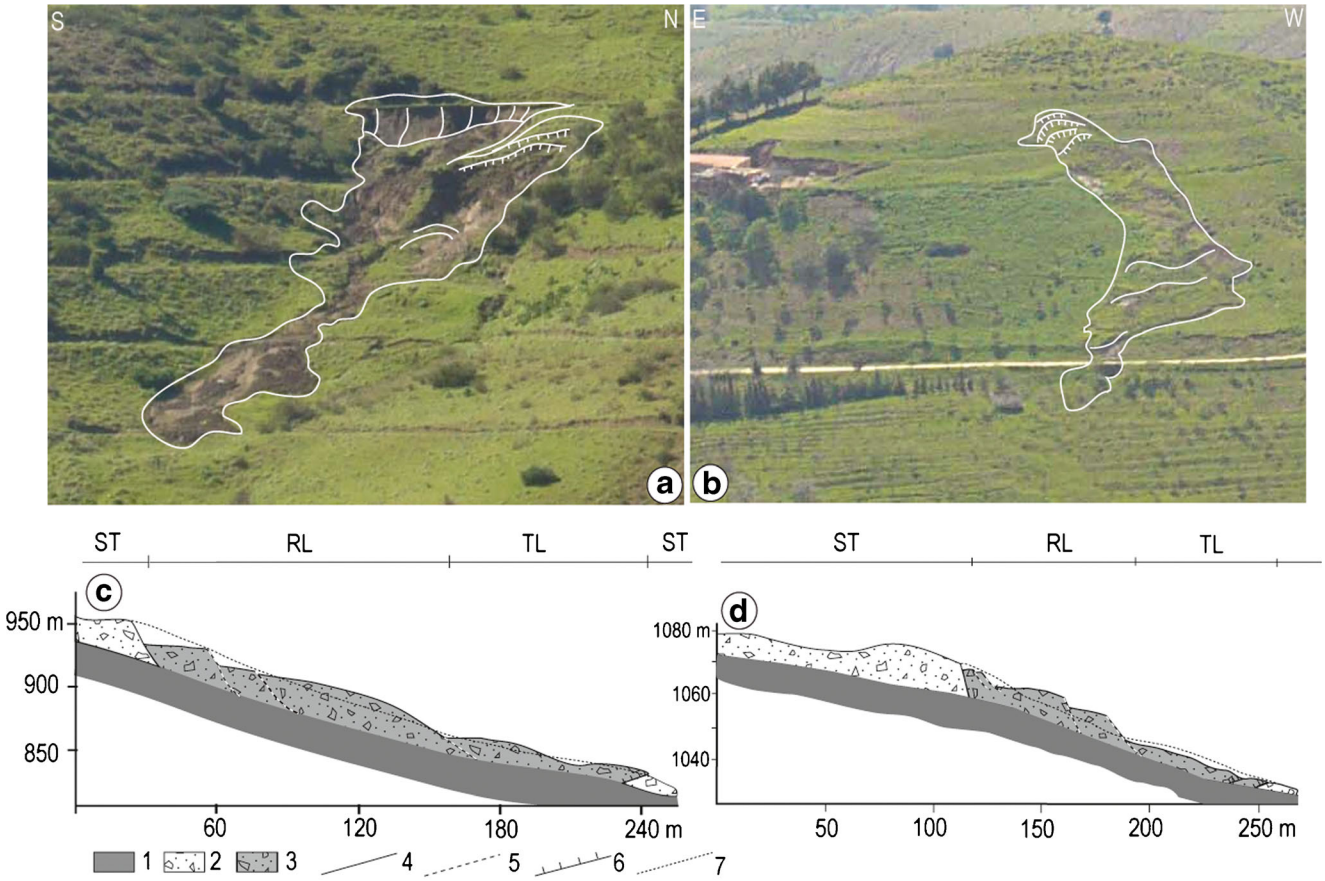

Fig. 6 Photographs showing complex translational and mixed translational and rotational landslides. **a** Landslide corresponding to the L39 event and **b** the L40 event. Both landslides are located in the southwest and west Bordj Bou Naâma, respectively. *White dashed lines* represent the area affected by the landslides, where rupture surfaces are clearly visible; **c**, **d** block diagram of both landslides, *ST* stable terrain, *RL* rotational landslide, *TL* translational landslide, *1* Albo-Aptian flysch, *2* colluviums in stable position, *3* destabilized material, *4* main rupture line, *5* secondary rupture line, *6* regression line on landslide, *7* initial topography

related to tectonic features, 10 of these are located related to the presence of roads, and 11 were related to catchment configuration. These landslides cover a total area of 0.27 km^2, representing 0.18 % of the total studied area.

Factor relationships

The maps give the locations and the properties of the past landslides. Since the slope failures are related to geological, topographical, and climatic conditions, it is important to determine the location and the contour of the landslide accurately in order to understand the relationships between the different factors (i.e., fracturing, slopes elongation, and water fluctuations). Morphologically, a landslide is characterized by two different zones: the first one is the rupture zone while the second one is the downstream accumulation area (Fig. 7c). In this figure, the (RA) axis represents the direction that matches the rupture planes while the (AA) axis is related to the accumulation zone along a direction parallel to the slope. A comparison was made to determine the importance of the disposition factors in relation to the triggered landslides. To do so, a statistical analysis was carried out to show a possible correlation between these factors for further modeling process. The analyzed fault lineaments were compared to the initial snatching lines and they represent ruptures planes. All maps related to topographic, tectonics faults, and water circulation are finally superposed in order to determinate the frequency of landslide.

Friction coefficient assessment

It has been shown that the H/L ratio where H is the difference of height and L is the horizontal length of the entire landslide provides valuable information regarding the landslides mobility (Scheidegger 1973; Hsü 1975). The effects of the topography on the H/L ratio have been observed by previous authors as well (Cruden and Varnes 1996; Finlay et al. 1999; Hunter and Fell 2003; Okura et al. 2003). The experimental and numeric studies have also shown that the H_i/L_i ratio, where H_i represents the height difference and L_i the length of the rupture area, controls the stopping zone of the moving

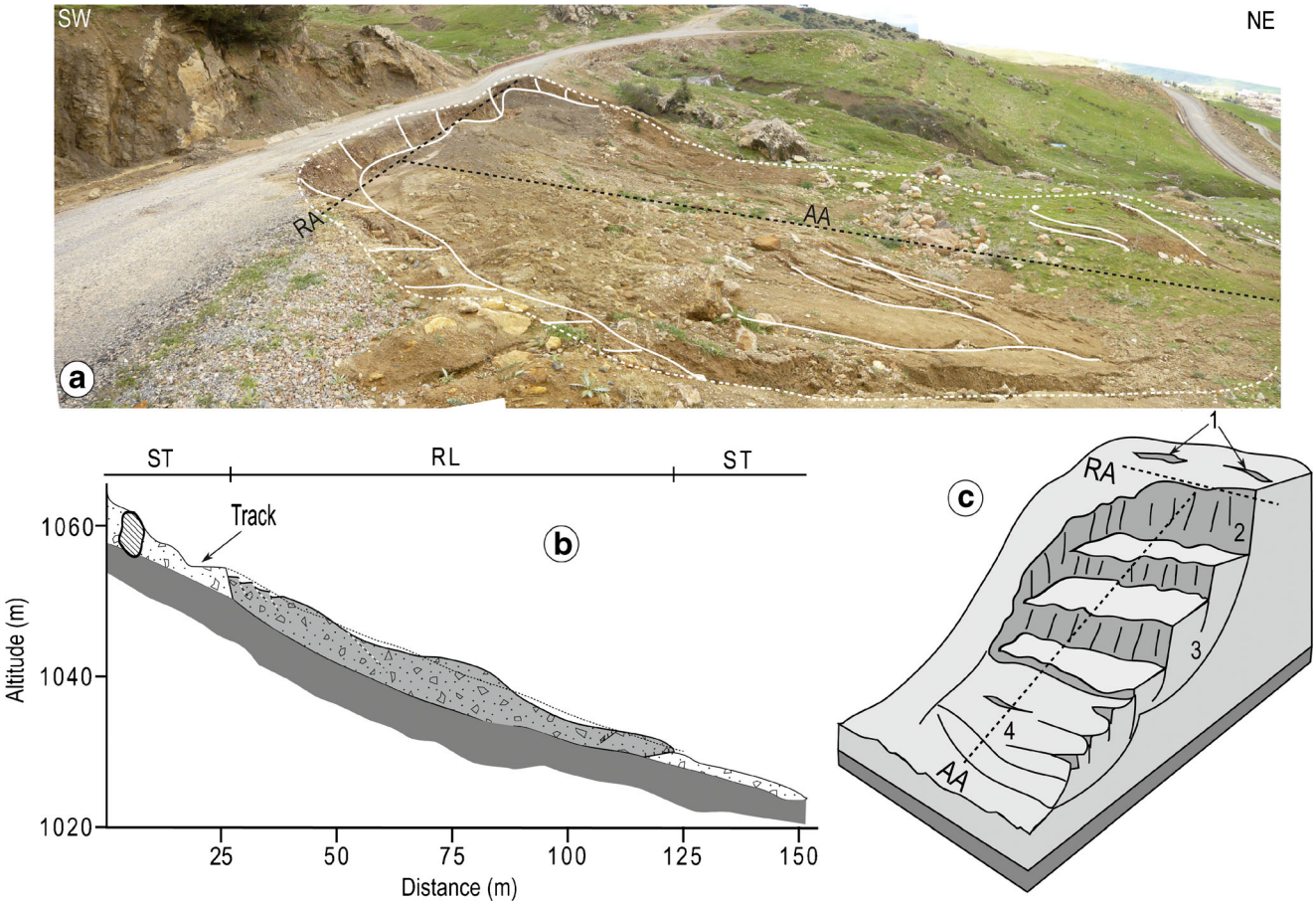

Fig. 7 Photographs of a rotational landslide (L36) in the north of Bordj Bou Naama village. **a** Landslides affecting a road, the *white line* shows the limits of landslides, the *vertical white line* shows the principal rupture surfaces and in the lower zone, flowing fluids were visible; panel **b** shows the corresponding diagram block in 2D; for this landslide, please refer to Fig. 6 for the abbreviations; **c** 3D diagram block showing the different parts of the rotational landslide with *1* sheet cracks, *2* main rupture surface, *3* secondary rupture surface, *4* debris flow area, *AA* debris flow accumulation axis, *RA* rupture axis. H_i height difference, L_f accumulation length, L_a rupture length. For abbreviations, refer to Fig. 4

granular mass along the horizontal plane (Corominas 1996; Chigira and Yagi 2006).

From these previous studies, the retained coefficient for this study involves the two morphometric indices: H_i which represents the difference between the maximum and the minimum height of landslide and L_f which characterized the length of the accumulated area (Fig. 7c).

Dynamic analysis

The most important part of the slopes stretches from the summit to the foot of the lithological contact, and it often exceeds 70 % of the total length per location (Fig. 6a). These high dip angle value slopes represent about 6.5 % of the total landslide area. Outside the steep zone, 72.6 % of the slopes are characterized by moderate values (25 %) (Fig. 8a). The slopes are mostly north or south oriented because of the west–east direction of the main structural units (Fig. 8b). Indeed, Sra Abdelkader elongating from west to east for 4 km presents most of the slopes elongated in the culminating area. Belkheiret and its satellites (Batha and Fartas) are orthogonally oriented from the Sra Abdekader massif (Fig. 8b). The summit lines of these structures trace a boundary between the WNW- and the ESE-oriented slopes for the eastern and western sides, respectively. However, their accumulative surfaces constitute only a small part of the entire area (Fig. 8b).

At lower altitude (i.e., under 1,000 m), the geological formations are represented by colluviums and turbidities with variable thicknesses (<10 m), which are ductile materials highly vulnerable to erosion processes. These materials overcome the Cretaceous flysch which are also slope oriented. It is important to note that the disposition of the slopes is accommodated by the local structure of the massif. This actual morphological configuration is the result of a Tortonian to Pliocene tectonic polyphase. The triggering mode of the landslides identified in these zones, whether it is rotational or translational, is accommodated by the tectonic or morphological knickpoints, respectively. The superposition of the

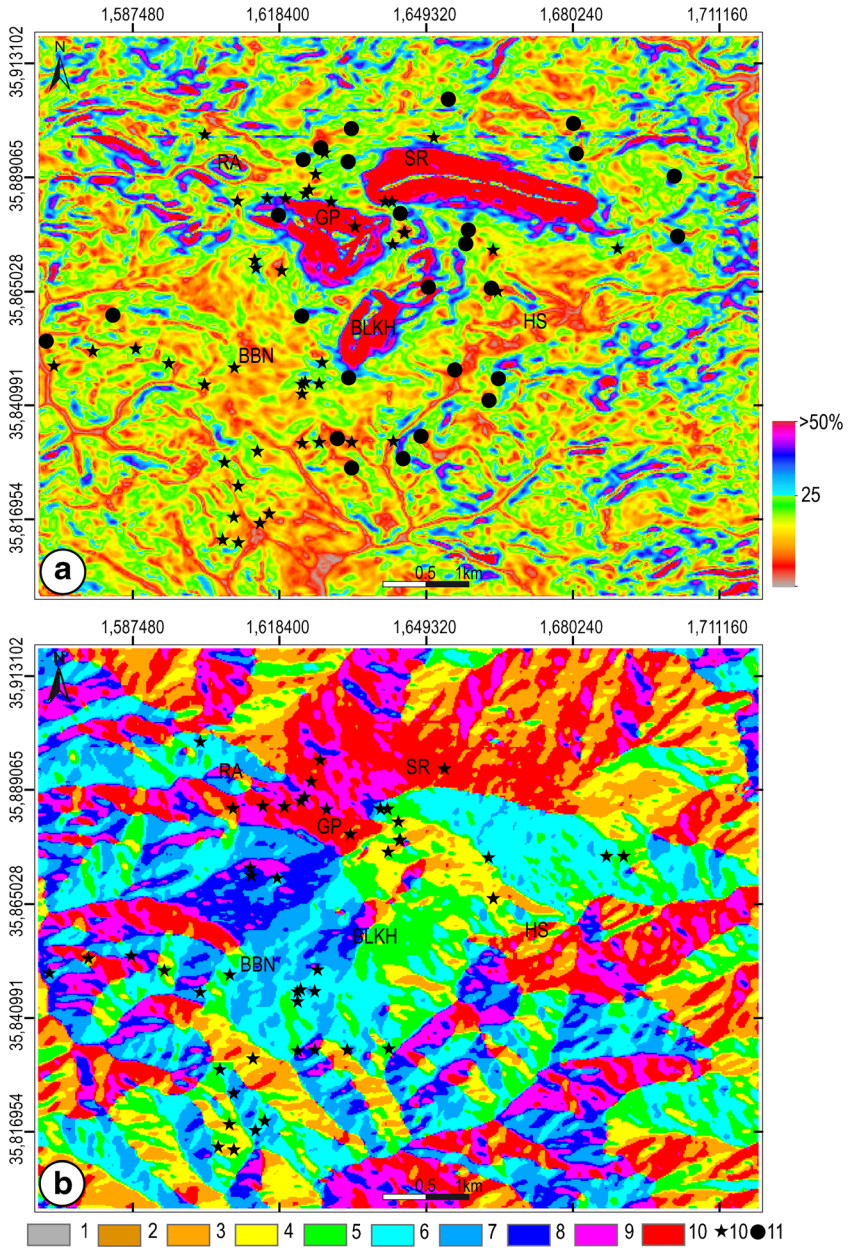

Fig. 8 Morphological characteristic of the culminating area: **a** slope map (%) and **b** aspect map, both are extracted for DEM (digital elevation model obtained for ASTER GDEM 2010): *1* flat, *2* north (0–22.5°), *3* northeast (22.5–67.5°), *4* east (67.5–112.5°), *5* southeast (112.5–157.5°), *6* south (157.5–202.5°), *7* southwest (202.5–247.5°), *8* west (247.5–292.5°), *9* northwest (292.5–337.5°), *10* north (337.5–360°), *11* circles represent the position of the different landslides identified in the Ouarsenis area, *12* asters showing the position of principal water sources. *BBN* Bordj Bou Naama, *SS* Hammam Sidi Slimane

inventory map of the landslides with the slope map shows that the majority of these instabilities appear in a slope ranging from 11 to 34 % (Fig. 9a. The superposition of slopes map on the water source map shows that groundwater fluctuations are also located in this type of slope, i.e., ranging from 11 to 22 % (Fig. 8a). These fluctuations are ensured by a complex exchange system (storage and karst water circulation). Indeed, limestone favored by intense fracturing and internal chemical dissolution acts as water storage areas (karst system) (Fleury et al. 2007). This water flow occurs through preexisting fractures in the basements and by gravity. This highly fractured Jurassic carbonate system helps to hydraulically load the karst from snowfall (Goldscheider 2005): these volumes of water are stored before flowing throw the marl layer underlying the fractures zone. This lithologic formation is characterized by frit facies (marl with shale appearance). Comparing the two graphics curves presented in (Fig. 9a), it can be seen that ~54.34 % of the landslides are located on slopes ranging from 11 and 22 %, where the water sources are localized (almost ~57 % of these sources are present on these soft slopes).

The set up landslide data base shows that more than 25 % of the landslides affect wetland areas with high water saturation degree. These soils are located on NW-, N-, and NE-oriented slopes (Fig. 9b); they are characterized by low sun heat accumulation. These slopes correspond to the northern slopes of the Grand Pic and the Rosfet Hallayeg Mount (HR) situated on the west side of BBN (Fig. 2b). In addition, more than 15 % of the landslides concern N180-225°-oriented

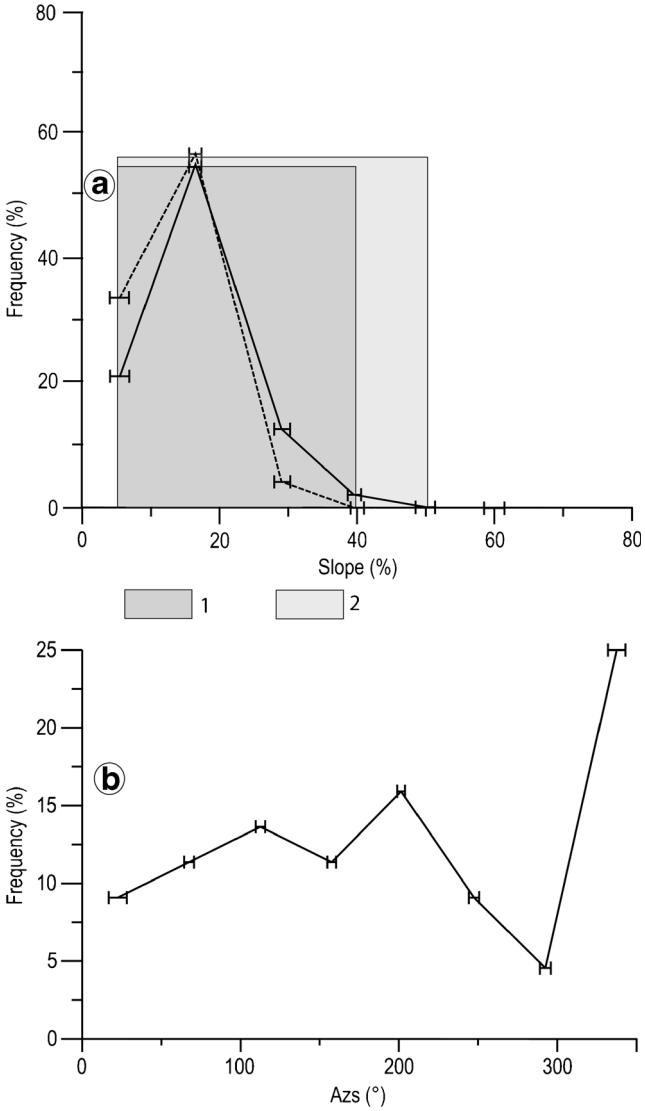

Fig. 9 Resulting dynamic parameters in the culminating area. **a** Landslides (*full line*) and fluids circulations (*dashed line*) frequency vs. topographic slopes; horizontal standard deviations (±2σ) refer to slope uncertainties; *1* and *2* represent maximum landslides frequency and maximum fluids circulations, respectively; **b** landslides frequency vs. slope azimuths (Azs); horizontal standard deviations (±2σ) refer to slope azimuths uncertainties

slopes, located in the southern side the Belkheiret massif. The results show that the initial rupture orientation of the landslides largely coincides with tectonic lineaments. Indeed, the current directions of tectonic fractures are oriented as follow: (i) N10°, which corresponds to a senestral strike slip process presents in the western part of Sra Abldekader as well as a reverse fault related to abnormal tectonic contact in the west of Belkheiret; (ii) N40°, which corresponds to a dextral strike slip process presents in the north of Grand Pic; and (ii) N80°, which correspond to the senestral strike slip process identified in the central part of the culminating area as well as a N160° direction corresponding to the well-known strike slip process affecting the western extremity of Sra Abdelkader zone (Fig. 10a). The lineaments related to the rupture zone (RA) have about the same directions (Fig. 10b). The representative rose diagrams of the landslides lineation coincides with the most active tectonic azimuths (Fig. 10b). More than 30 % of landslides are oriented N40° and N120°. At the tectonic scale, the majority of these two directions characterize: (i) the highest zones of Rokba Atba, Belkheiret, Grand Pic, and Sra Abdelkader massifs; (ii) the central part of area culminating. It has been observed that the faults directions and the lineaments of landslides represented by a rupture zone (RA) (Fig. 7c) have a likelihood of 73.80 % (Fig. 10a, b), whereas the accumulation area (AA) direction of the landslides (i.e., flow destabilized materials) is different (Fig. 7c). Indeed, they show low likelihood values, especially for N30° and N160° directions (Fig. 10c).

Morphometrics analysis

The results also show that the landslide located right after the tectonic knickpoint line presents a negative slope for the linear fitting (Fig. 11a), and the accumulation area lengths are reduced (Fig. 11a and Table 3). All of these landslides have a coefficient of friction ranging from 0.15 to 0.5, as the displacement lengths do not exceed 200 m (Fig. 9a and Table 3). When considering the overall landslides, the average value of this coefficient rises to ~0.24. The landslides located in the opposite direction of the tectonic contacts have an important displacement length and they can reach 700 m at some places (see Table 1). They mainly affect catchment zones with normal lithological concordance. Their corresponding coefficient of friction is about 0.25 (Fig. 11b). In the case of landslides presenting a fluid flow behavior, the observations indicate that the length of the deposition zones is very important (Fig. 6a, b). The linear fitting corresponding to these cases also presents a negative slope (Fig. 11c) with a coefficient of friction (H_i/L_f) about 0.23 (Table 3), it is almost the same results in the case of landslide located beyond the tectonic knickpoint slope with 0.24 of FoS. However, the landslides with no water seepage show a higher coefficient of friction (0.29), and a significant percentage of this type of landslides has the same length range of displaced materials, with the relative linear fitting exhibiting a positive slope (Fig. 9d).

Results and discussions

It has been found that a relationship exists between the location of the landslides, the type of phenomenon, and the local geomorphologic characteristics of the area. Indeed, the distribution of unstable slopes seems to be strongly dependent on the existence of tectonic faults overlapping structures. Along these faults, also called abnormal contacts, the structural units

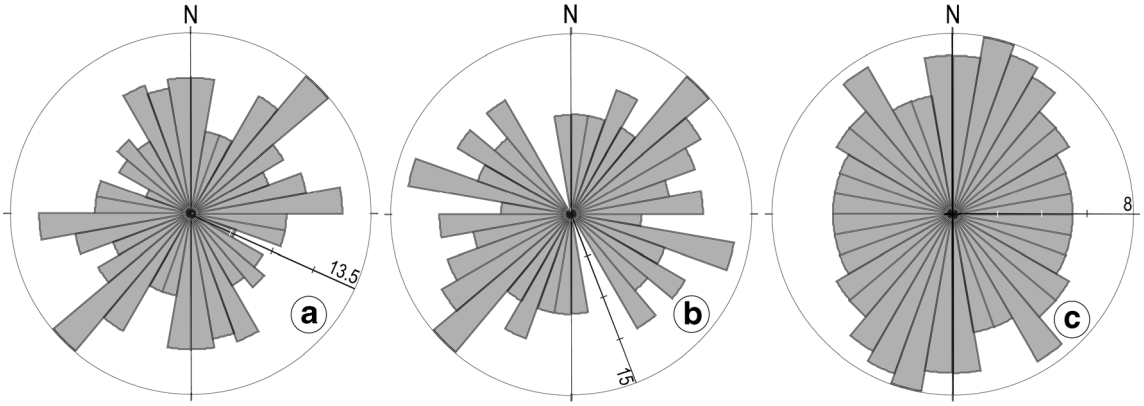

Fig. 10 Rose diagrams of normalized (in %): **a** fault directions; **b** landslide azimuths; and **c** slope surfaces elongation

are exhumated during the early compressive tectonic phases. This led to the current geomorphology characteristics. The underlying formations pierced all allochtonous and autochthonous series. It results in very hard Jurassic formations overlapping the lower Cretaceous turbidity. These carbonate formations are the seat of a significant water storage from snowfall occurring at high altitudes (over 1,000 m). The successive deformation has also created chaotic slopes on the front of the overlap. However, the catchment located in the "background" of these overlap liner has homogeneous concave slopes. The distribution of groundwater coming from the karst systems is favored by the presence of fractured rock masses. Since water is present all the yearlong in weak materials, these areas present a very unstable configuration.

A relationship between the dynamic and the morphometric indices for landslides at the catchment scale has also been found. The results show that the majority of landslides are located on gentle slopes that do not exceed 34 %. The superposition of areas represented by fluid flow activity associated to different classes of slopes showed that 56 % of the water springs are located on slopes that do not exceed 22 % (Fig. 9a). The majority of these areas are characterized by weak materials. It appears from these results that these ranges of slopes are affected by the majority of landslides with a percentage 54.34 %. The corresponding coefficient of friction values range from 0.15 to 0.5. This can be explained by the fact that the same morphologic conditions are involved. The majority of these landslides affect superficial formations material overlying ductile ones (Aptian-Albian Flysch units). An exception is made with a landslide affecting a stadium (L5 case) (Fig. 4a) (Table 1). In this case, the tomographic profiles indicate that the deep underlying formations (schist) are also affected by the rupture process.

The overlying colluviums, present in the culminating zones, are also highly vulnerable to slope instability. These sides of the culminating zone are subjected to the same boundary conditions. Morphological particularities are different from one side to another. They present different topography, i.e., concave/convex and concave geometry. The fluid flow is controlled by a draining system as well as fracture

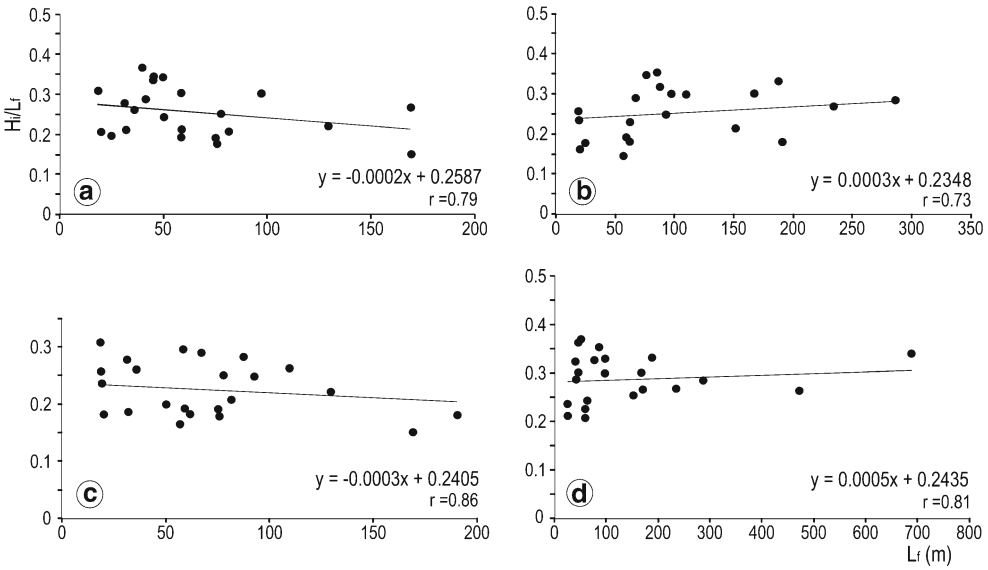

Fig. 11 Friction coefficient H_i/L_f ratio vs. L_f for different landslides. **a** Tectonic slope rupture; **b** geomorphologic slope rupture; **c** fluid circulations occurrence; and **d** no apparent fluid circulations. H_i altitude drop (m); L_f debris flow accumulation distance (m)

corridors present in ductile materials. The displacement length of the materials is more important in localized areas beyond the geomorphologic knickpoints. One consequence is that the slopes are more elongated and have a concave appearance as seen, for example in the Southern part of Sra Abdelkader area. Landslides accommodated by a knickpoint related to tectonic contact present short spread lengths. Indeed, these slopes located on the mountain side highly affected by tectonic contact; they have a chaotic character. Most of the landslides presenting these characteristics are NW-, N-, and NE-oriented slopes (Fig. 9b). These slopes surfaces are have a low sun heat input (Soltner 1992). This orientation reduces the evaporation rate, keeping a high water content in the colluviums layers which contain a high percentage of clays coming from the bedrock (flysch units). Thus, this fully saturated material is highly vulnerable to gravitational instability.

The recent data showed that the culminating zone was affected by two compressive phases during the Cenozoic. These phases have produced folds NW/SE- and NE/SW-oriented direction (Zaagane et al., Comptes Rendus of Geoscience, under review). The induced fracturing process is represented by neoformed faults of radial form with different directions (N10° N40°, N80, and N160° orientations). This structuration has played a crucial role in the accommodation of schistosity in ductile materials (Fig. 10). The landslide triggering is mainly related to the primary cracking of the tectonic fracturing. Indeed, the direction of the ruptures surfaces (RA) (Fig. 7c) compared to the direction of the tectonic fracturing lineaments shows a good agreement. Thus, the majority of the ruptures lines of landslides orientations are ranging from N15° to N110° directions (Fig. 10a). The rose diagrams of the tectonic faults show that the mains directions are N45, N90, N120, and N160° oriented (Fig. 10a). As mentioned previously, these faults direction are related to the two compressive phases (Zaagane et al., Comptes Rendus of Geoscience, under review) and it has been seen that 78 % of the fault directions coincide with the main landslide rupture line (Fig. 10b). It can be conclude that the recent tectonic event accommodate most of the landslide rupture line. This finding is clearly observed by the parallelism of the rupture line of L5 landslide with the major fault located in the southern part of Belkheiret (N140°). The elongation axis of the large slopes corresponds to the preferential direction of the landslides (ruptures axis). Only one unique case exhibits a different direction (N160°).

These results leads us to suggest that the resulting fracturing process generated by recent tectonics phases is at the origin a secondary crack field present in the ductile material, thus driving the line direction of initial rupture of landslides. It turns out that the size of the large slopes plays a secondary role in this process. Only the topographic slope gradient remains an essential element not only in triggering these instabilities but also the spreading of the destabilized materials.

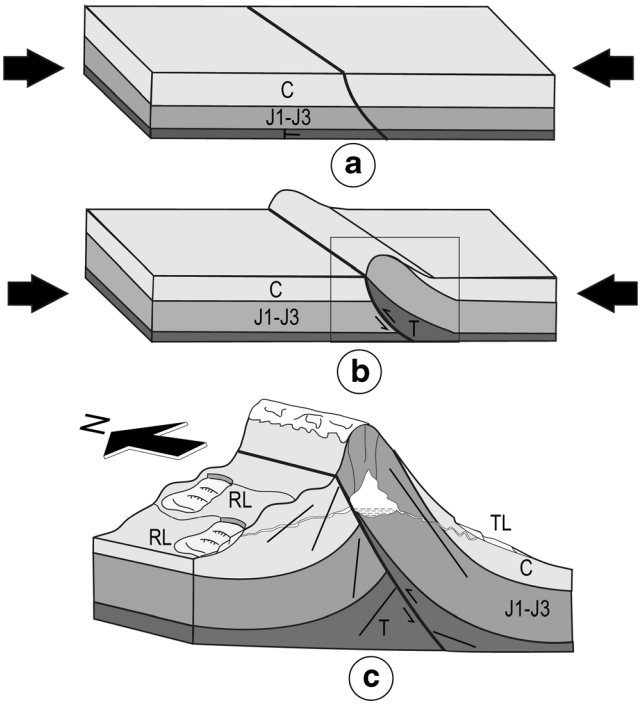

Fig. 12 Conceptual model of landslide localization in the Ouarsenis culminating zone. *Large arrows* represent the stress regime direction during thrusting: **a** faulting initiation; **b** thrusting; **c** thickening by a stack of nappes and slope deformation at the final stage causing rotational (*RL*) and translational (*TL*) landslides. This model can be applied to nearly all massifs but not to GP since it is composed of para-autochtoneous series. Same notations as in Fig. 2

Conclusions

The current geomorphologic face of the Ouarsenis area is the direct result of a complex and polyphase tectonic processes. The late compressive tectonic stress-oriented NW/SE NNE/SSW, and NE-SW can be related to the late Miocene, the late and upper Pliocene, respectively. This structuring led to the establishment of a very craggy relief (Fig. 10a). The maximum shortening is estimated to be about 300 m. Therefore, the exhumation of this relief generates strong topographic anomalies; it is the seat of abundant material transfers whose gravitational instabilities belong. Lines of tectonic contacts marked weak boundaries along these extruded reliefs (Fig. 11b). This extrusion generated a chaotic topographic form represented by short slopes (concave-convex), increasing the vulnerability of catchment areas to slip phenomena.

Our study shows that the average coefficient of friction of the identified landslides has a value of 0.24. This value corresponds to landslides identified beyond the tectonic contact knickpoint (in the sense of the massifs spill). These slopes are short, involving a minimum volume of destabilized material. However, the geomorphologic slopes have a concave form and spread over long distances. For this type of slopes, the destabilized material represents a large volume; this could

be justified by a higher coefficient of friction (0.25). This assumption was confirmed by a percentage of 38.09 % of translational slides located in the eastern part of the Ouarsenis, which is characterized by a geomorphologic knickpoint.

These landslides are related to long slopes with a lithological concordance of same directions; however, the western part of the culminating area is characterized by 86.95 % of rotational landslides type related to chaotic slopes.

The Jurassic calcareous massifs play an essential role in the water storage from snow melting. They occupy a culminating position and they were subjected to an intense fracturing process (tectonic, thermoclastic, and chemical cracking). These fractured rock masses provide water channels, feeding a steep complex karst system, giving rise to an intense fluid flow activity (Fig. 12c). The circulation of those fluids generates several potential downstream water springs. The fluid flow in a granular and laminated environment, i.e., colluviums and flyschs, is the main cause of the gravitational instabilities. As well known, the results show a lower friction coefficient value in a wet environment than in a dry one 0.23 and 0.29, respectively. For saturated cases, the materials are easily destabilized and slip even if the slopes are gentle (Stadium landslide L5 case) (see Table 1).

It appears from these results that the culminating zone of Ouarsenis was the seat of a young tectonic post-Tortonian activity (<11 Ma). This active and continuous tectonic process generated craggy massifs. These structural units were exhumated along the abnormal tectonic contact. The late phase is responsible of a radial fault distribution:

- The first folding generated the N160°, N140°, and N120° faults, located in the western part of Sra Abdelkader, Chicot massif, Rokba Atba, and The Grand Pic.
- The second folding generated the N40°, N80°, N120°, and N140° faults located in the south (Belkheiret, Fartas, and Batha).

This fault distribution accommodates the apparition of "fracturing" landslides favored by (i) a vulnerable lithology and (ii) the presence of fluid circulation. At these predisposing and climate factors, a seismic activity parameter could be added. Note that this area is situated near the Chlef region characterized by very important earthquake events (e.g., destructive earthquake with 7.3 on the Richter scale which occurred in 1980). At that time, people witnessed rock block collapse from limestone massifs.

Finally, it is important to enhance the fact that anthropogenic factors caused by (i) buildings in zone with high hazard level, (ii) destruction of the vegetal cover (deforestation), and (iii) vibration causing by transport and mining activity induce high susceptibility to landslides.

It has been strengthen in the present study that the groundwater coming from karst zone (limestone massifs) plays a major role in easing landslide and major effort in well-designed and efficient draining systems could be undertaken. Doing so, the impact of sliding under the effect of saturated ground could be minimized. The establishment of a detailed hazard map becomes mandatory in order to set up the risk assessment.

Acknowledgments The authors are indebted to the anonymous reviewer for the constructive remarks which helped improve the final version of the manuscript. The authors wish to thank the local village authorities of Bordj Bou Naama for ease of access in the field as well as the availability under our all documents necessary for the preparation of this work. One of the authors would like to thank the regional project Mistrals "ENVI-MED."

References

Adushkin VV (2000) Explosive initiation of creative processes in nature. Combust Explosion Shock Waves 36(6):695–703

Atrops F, Benest M, Almeras Y, Benosman B (1991) Découverte et dynamique d'une transgression au Callovien sur le socle tardi-hercynien dans le domaine sud-tellien (Ouarsenis, Algérie). C R Acad Sci Paris 313(13):1555–1562

Benaouali-Mebarek N, Frizon de Lamotte D, Roca E, Bracène R, Sassi W, Faure J-L, Roure F (2006) Post-Cretaceous kinematics of the Atlas and Tell systems in Central Algeria: early foreland folding and subduction-related deformation. C R Geosci 338:115–125

Benhamou M (1996) Evolution tectono-eustatique d'un bassin de la Téthys maghrébine: l'Ouarsenis (Algérie) pendant le Jurassique inférieur et moyen. Thèse de Doctorat ès Sci., Université d'Oran, 434p

Benhamou M, Elmi S, Alméras Y (2000) Age et contexte dynamique des calcaires à brachiopodes téthysiens (Zeilleriidés multiplissés) du Grand Pic de l'Ouarsenis (Tell algérien). C R Acad Sci Paris 331: 717–723

Blès J-L (1971) Étude tectonique et microtectonique d'un massif autochtone tellien et de sa couverture de nappes: (le massif de Blida, Algérie du Nord). Bull Soc Géol France 13(5–6):498–511

Bouillin J-P, Durand Delga M, Gélard J-P, Leikine M, Raoult JF, Raymond D, Tefiani M, Vila J-M (1970) Définition d'un flysch massylien et d'un flysch maurétanien au sein des flyschs allochtones de l'Algérie. C R Acad Sci Paris t. 270:2249–2252

Calembert L (1952) Etude géologique du Massif culminant de l'Ouarsenis. Bull Serv Carte Géol Algérie 2(23):184p

Carrara A, Cardinali M, Detti R, Guzzetti F, Pasqui V, Reichenbach P (1991) GIS techniques and statistical models in evaluating landslide hazard. Earth Surf Process Landf 16:427–445

Carrara A, Crosta G, Frattini P (2003) Geomorphological and historical data in assessing landslide hazard. Earth Surf Process Landf 28: 1125–1142

Chigira M, Yagi H (2006) Geological and geomorphological characteristics of landslides triggered by the 2004 Mid Niigata prefecture earthquake in Japan. Eng Geol 82:202–221

Corominas J (1996) The angle of reach as a mobility index for small and large landslides. Can Geotech J 33:260–271

Cruden DM, Varnes DJ (1996) Landslide types and processes. In: Turner AK, Schuster RL (eds) Landslides: investigation and mitigation (Transportation Research Board Special Report No. 247). National Academy Press, Washington, pp 36–75

Dade WB, Huppert HE (1998) Long-run out rockfalls. Geology 26:803–806

Dalloni M (1936) Matériaux pour l'étude géologique du massif de l'Ouarsenis. Bull Serv Géol Algérie 2(13):41p

DurandDelga M (1969) Mise au point sur la structure du Nord-Est de la Berberie. Bull Serv Carte Géol Algérie 39:89–131

Elmi S, Alméras Y, Benhamou M, Mekahli L, Marok A (2003) Biostratigraphie des brachiopodes et âge carixien (Pliensbachien inférieur) des calcaires à grands bivalves en Algérie occidentale. Geobios 36(6):695–706

Farès Khodja F (1968) Contribution à l'étude stratigraphique et micropaléontologique du jurassique du Tell algérien (massif culminant de l'Ouarsenis, Oued Fodda et les massifs de la plaine du Chélif-Babor). Thèse 3ème cycle, Faculté des Sciences de Paris, 166p

Finlay PJ, Mostyn GR, Fell R (1999) Landslide risk assessment: prediction of travel distance. Can Geotech J 36:556–562

Fleury P, Plagnes V, Bakalowicz M (2007) Modelling of the functioning of karst aquifers with a reservoir model: application to Fontaine de Vaucluse (South of France). J Hydrol 345(1):38–49

Glangeaud L (1951) Interprétation tectonophysique des caractères structuraux et paléogéographiques de la Méditerranée occidentale. Bull Soc Geol Fr 6(1):735–762

Goldscheider N (2005) Fold structure and underground drainage pattern in the alpine karst system Hochifen-Gottesacker. Eclogae Geol Helv 98(1):1–17

Guthrie RH, Evans SG (2004) Analysis of landslide frequencies and characteristics in a natural system, coastal British Columbia. Earth Surf Process Landf 29:1321–1339

Hattanji T, Moriwaki H (2009) Morphometric analysis of relic landslides using detailed landslide distribution maps: implications for forecasting travel distance of future landslides. Geomorphology 103(3):447–454

Hsü KJ (1975) Catastrophic debris streams (Sturzstroms) generated by rockfalls. Geol Soc Am Bull 86:129–140

Hunter G, Fell R (2003) Travel distance angle for "rapid" landslides in constructed and natural soil slopes. Can Geotech J 40(6):1123–1141

Kireche O (1993). Evolution géodynamique de la marge tellienne des Maghrébides d'après l'étude du domaine parautochtone schistosé (massifs du Chélif, d'Oranie, Bou Maâd, des Babors et des Bibans). Thèse de Doctorat, Université d'Alger, 316p

Lebuis JR, Robert JM, Rissman P (1983) Regional mapping of landslide hazard in Quebec. Proceedings of the International Symposium on Slopes on Soft Clays, Linkoping, Swedish Geotechnical Institute. Report 17:205–262

Lucas A, Mangeney A (2007) Mobility and topographic effects for large Valles Marineris landslides on Mars. Geophys Res Lett 34, L10201

Lucas A, Mangeney A, Bouchut F, Bristeau MO, Mège D (2007) Benchmark exercises for granular flows. The 2007 International Forum on Landslide Disaster Management, Ho and Li, 2:967–986

Lucas A, Mangeney A, Mège D, Kelfoun K (2008) New methodology for initial volume estimation of Martian landslides from DTM and imagery. Workshop on Martian Gullies: Theory and Tests, Houston, TX., 8023

Lucchitta BK (1987) Valles Marineris, Mars-Wet debris flows and ground ice. Icarus 72:411–429

Mangeney A, Bouchut F, Thomas N, Vilotte J-P, Bristeau M-O (2007) Numerical modeling of self-channeling granular flows and of their level channel deposits. J Geophys Res 112, F02017

Mangeney-Castelnau A, Bouchut F, Vilotte JP, Lajeunesse E, Aubertin E, Pirulli M (2005) On the use of Saint Venant equations to simulate the spreading of a granular mass. J Geophys Res 110, B09103

Maquaire O, Weber C, Thiery Y, Puisant A, Malet JP, Wania A (2004) Current practices and assessment tools of landslide vulnerability in mountainous basins. Identification of exposed elements with a semi-automatic procedure. Proceedings 9th International Symposium on Landslides, Leiden, Balkema: 171–176

Martha TR, Kerle N, Jetten V, van Westen CJ, Kumar KV (2010) Characterising spectral, spatial and morphometric properties of landslides for semi-automatic detection using object-oriented methods. Geomorphology 116(1):24–36

Mattauer M (1958) Etude géologique de l'Ouarsenis oriental (Algérie). Bull Serv Géol Algérie, Monogr Régionale 17:534p

Meghraoui M, Pondrelli S (2013) Active faulting and transpression tectonics along the plate boundary in North Africa. Ann Geophys 55(5), doi:10.4401/ag.4970

Okura Y, Kitahara H, Kawanami A, Kurokawa U (2003) Topography and volume effects on travel distance of surface failure. Eng Geol 67: 243–254

Polvèche J (1960) Contribution à l'étude géologique de l'Ouarsenis oranais. Bulletin des Services de la Carte géologique de l'Algérie, Bulletin 24(I,II), 577p

Raoult JF (1974) Géologie du centre de la chaîne numidique (Nord du Constantinois, Algérie). Mém.Soc. géol. France, N.S., t. III, n° 121, 164 p

Scheidegger AE (1973) On the prediction of reach and velocity of catastrophic landslides. Rock Mech 5:231–236

Soltner D (1992) Les bases de la production végétale le sol, le climat, la plante Tome II, Le climat, 6ème édition. Collection sciences et techniques agricoles. 320p

Tchoumatchenco P, Nikolov T, Kozhukharov D, Benev B, Gochev P, Katzkov N, Khrischev K, Moev M, Nicolov Z, Slavov I, Tzankov T, Zidarov N (1995) Le Crétacé inférieur dans le massif de l'Ouarsenis et les Monts de Tiaret (Algérie du Nord). Geol Balc 25(2):27–59

Thiery Y (2007) Susceptibilité du bassin de Barcelonnette (Alpes du Sud, France) aux 'mouvements de versant': cartographie morphodynamique, analyse spatiale et modélisation probabiliste, Thèse de Doctorat, université de Basse Normandie, Caen, 445p

Thiery Y, Malet J-P, Maquaire O (2004) Observation on the activity of the Bois Noir landslide. Internal Report, EC-FP5 Alarm Project, Brussels. 10p

Thiery Y, Malet J-P, Sterlacchini S, Puissant A, Maquaire O (2007) Landslide susceptibility assessment by bivariate methods at large scales: application to a complex mountainous environment. Geomorphology 92:38–59

Wildi W (1983) La chaîne tello-rifaine (Algérie, Maroc, Tunisie): structure, stratigraphie et évolution du Trias au Miocène. Rev Géogr Phys Géol Dynam Paris 3:201–299